Molecular-scale mechanisms of crystal growth in barite

Carlos M. Pina, Udo Becker, Peter Risthaus, Dirk Bosbach & Andrew Putnis

Institut für Mineralogie, Universität Münster, Corrensstrasse 24, 48149 Münster, Germany

Models of crystal growth have been defined by comparing macroscopic growth kinetics with theoretical predictions for various growth mechanisms[1,2]. The classic Burton–Cabrera–Frank (BCF) theory[3] predicts that spiral growth at screw dislocations will dominate near equilibrium. Although this has often been observed[2,4], such growth is sometimes inhibited[4,5], which has been assumed to be due to the presence of impurities[6]. At higher supersaturations, growth is commonly modelled by two-dimensional nucleation on the pre-existing surface according to the 'birth and spread' model[7]. In general, the morphology of a growing crystal is determined by the rate of growth of different crystallographic faces, and periodic-bond-chain (PBC) theory[8,9] relates this morphology to the existence of chains of strongly bonded ions in the structure. Here we report tests of such models for the growth of barite crystals, using a combination of *in situ* observations of growth mechanisms at molecular resolution with

the atomic force microscope[10,11] and computer simulations of the surface attachment of growth units. We observe strongly anisotropic growth of two-dimensional nuclei with morphologies controlled by the underlying crystal structure, as well as structure-induced self-inhibition of spiral growth. Our results reveal the limitations of both the BCF and PBC theories in providing a general description of crystal growth.

Observations of crystal growth mechanisms were made in a fluid cell of a DI Multi-Mode atomic force microscope (AFM), using freshly cleaved, optically clear natural barite crystals as substrates. The surfaces studied were (001) and (210), the morphologically most important in barite[12]. We used X-ray diffraction to confirm the cleavage surfaces as (001) and (210) and to define crystallographic directions in the plane of the substrate. The unit cell of the barite structure[13] ($a = 8.87$ Å, $b = 5.45$ Å, $c = 7.15$ Å, space group *Pnma*) consists of two $BaSO_4$ layers parallel to (001), each layer related by a 2_1 screw diad axis parallel to *c*.

The cleaved (001) surface typically shows unit-cell high cleavage steps, and in Fig. 1a the cleavage surface intersects a screw dislocation line. At this point, such a cleavage step terminates. At the start of the experiment, deionized water was passed over the crystal, causing slight dissolution and the separation of the cleavage steps into half-steps (Fig. 1a). The presence of the screw dislocation allows spiral growth to be followed from the earliest stage and compared with two-dimensional nucleation.

A few seconds after injecting slightly supersaturated $BaSO_4$ solution, crystal growth begins. The cleavage steps migrate normal to their length and spiral growth begins at the dislocation core (Fig 1b, c). A new $BaSO_4$ layer spreads away from the core to one side but does not continue around the spiral as in classical descriptions of spiral growth[5]. Instead, the spiral becomes increasingly tightly wound around the core with very little lateral growth. Subsequently, a small number of two-dimensional nuclei, one $BaSO_4$ layer thick (3.6 Å), are formed on the surface. These nuclei are bounded by two straight edges parallel to ⟨120⟩ directions and a curved edge defining a sector shape (Fig. 1d). The nuclei on each alternate $BaSO_4$ layer are oriented in opposite directions, with those on a newly grown layer related by a 2_1 diad axis to those on the original cleavage surface (Fig. 1e). The growth of these nucleated islands is highly anisotropic, with growth normal to the curved edges being of the order of 10 times faster than growth normal to the straight edges. A fresh injection of more supersaturated solution into the fluid cell results in a higher nucleation density (Fig. 1f), but the lateral growth of the spiral remains very much slower than that of the two-dimensional nuclei, forming a small growth hillock.

The microtopographic features of the nuclei and the spiral on the barite (001) face indicate strong structural control of the growth process. Observations made on {210} cleavage surfaces of the same barite crystals show a very different growth morphology (Fig. 2). On the (210) barite surface, the nuclei grow as long needles that are one molecular layer thick (3.4 Å) along the ⟨1$\bar{2}$0⟩ directions. The growth rate is also highly anisotropic along the length of the needles, with growth being ~10 times faster along the [120] direction than in the opposite [1$\bar{2}$0] direction. Figure 3a shows the relevant crystallographic orientations on both barite surfaces.

These observations raise important questions relating to the

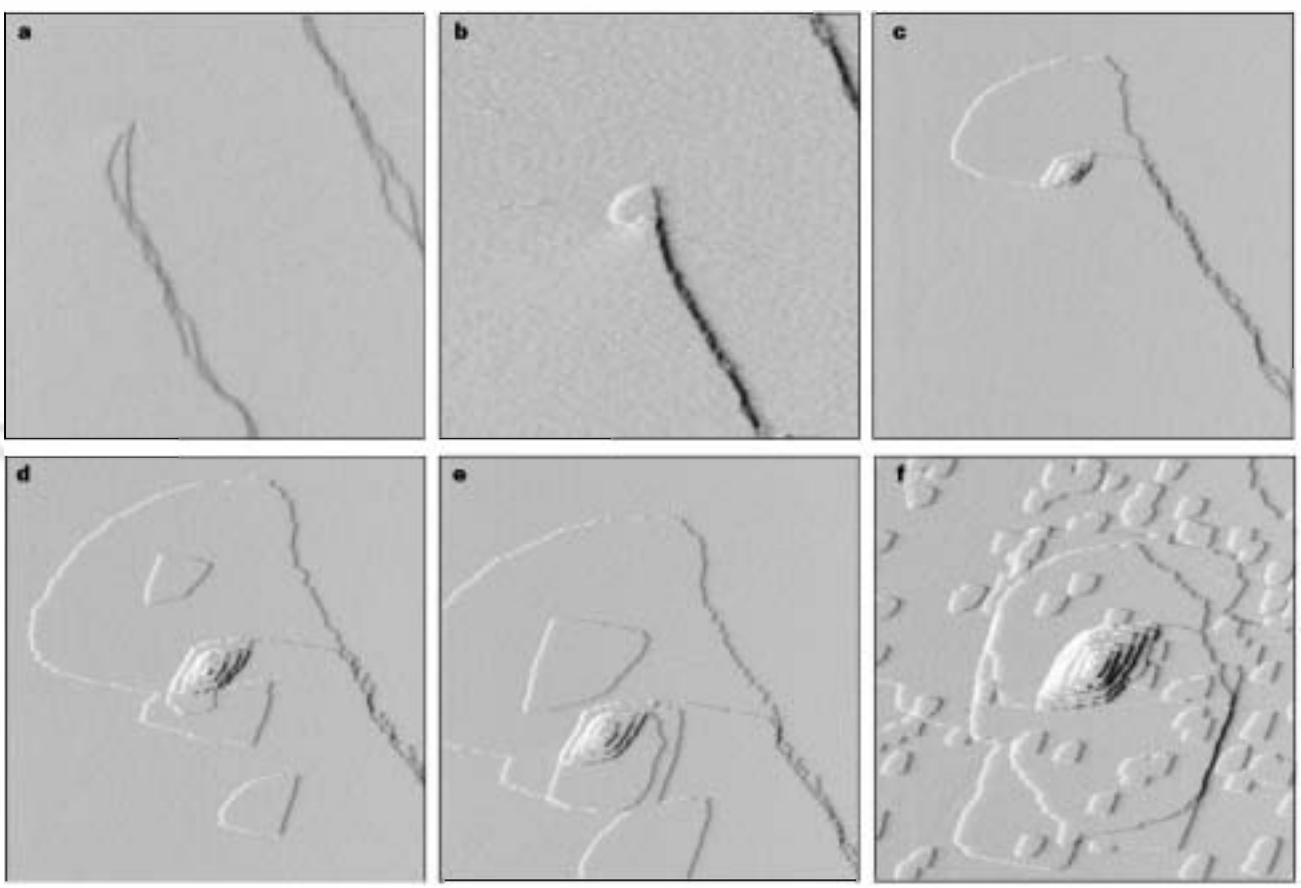

Figure 1 The crystal growth sequence on an (001) cleavage plane in a $BaSO_4$ solution with a supersaturation value of $a(Ba^{2+})a(SO_4^{2-})/K_{sp} = 12$. (Here *a* is the ion activity and K_{sp} is the solubility product.) **a**–**e**, Growth sequence over 60 min. Spiral growth begins at the dislocation core with the growth of a molecular layer of $BaSO_4$ (thickness, 3.6 Å), but subsequent lateral growth around the spiral is restricted. After ~40 min, during which fresh fluid is pumped over the sample, two-dimensional nucleation begins (**d**), with a nucleation density of ~0.12 nuclei per μm^2. Note the opposite orientation of the sector-shaped nuclei. **f**, After 85 min of growth, a fresh injection of solution with a supersaturation value of 26 results in a greatly increased nucleation rate (~22 nuclei per μm^2). The image area in each case is 2 μm × 2 μm.

crystal growth process, none of which can be adequately addressed using current theories. What determines the shape of the two-dimensional nuclei, why is their growth so anisotropic, and what inhibits the lateral growth of the spirals?

The prediction of crystal growth morphology is based on the concept that crystal faces contain different numbers of chains of nearest-neighbour bonds, or PBCs (periodic bond chains)[8,14]. PBC analysis can also provide information about the surface morphologies on F-faces[15], which contain two or more such PBCs and can grow by a layer mechanism. Both (001) and (210) are F-faces and PBC theory explains the layer-by-layer mechanism and the thickness of the growth layers: half-unit cell for (001) and one unit cell for (210) faces[9,16]. In addition, needles on (210) and the straight edges of the sector-shaped nuclei on (001) are parallel to ⟨120⟩, which are directions of strong PBCs. However, as PBC theory was designed to deal with periodic systems and not with the attachment of single molecules at specific surface sites, it is necessary to apply molecular modelling techniques to explain the anisotropy of the growth along the PBCs and the existence of the curved edge.

We used ionic models incorporated in Cerius2 (Molecular Simulations, BIOSYM) and GULP (J. Gale, Imperial College, London) with potentials similar to those derived in ref. 12, but slightly modified to model the lattice energy of barite better. All values for attachment energies were corrected for the hydration energies of the respective ions (Ba^{2+}: 13.7 eV (ref. 17); SO_4^{2-}: 9.8 eV derived from ref. 18). Starting the stimulation with the most energetically favourable nucleus of two Ba^{2+} and two SO_4^{2-} ions (outlined as the small rhombohedron in Fig. 3b), we first calculated the attachment energies for both species at their respective lattice positions around the step edges of the nucleus. Attachment energies of SO_4^{2-} ions at positions **A** and **B** in Fig. 3b are endothermic at +3 eV and +4 eV respectively, but are more favourable than attachment of Ba^{2+} to this nucleus. Allowing the SO_4^{2-} ions to relax away from these lattice positions reduces the attachment energy, and ions from both **A** and **B** relax to a position close to position **A** with an attachment energy of +0.9 eV, clearly demonstrating the anisotropy of the attachment process. As this value is still positive, starting a new row along the [120] direction from **A** towards **C** is the rate-limiting step because the consecutive addition of further ions is exothermic and growth of each row continues towards position **C**. The same analysis was carried out after continued growth of the nucleus (**A′**, **B′**, **C′**). The energies for the attachment of Ba^{2+} ions to positions **D** and **E**, after adsorbing SO_4^{2-} to **A′**, are comparable, and therefore growth of a new row can be started from **E** before the row through **A′** and **D** is complete. This phenomenon of growing rows with different lengths leads to the shape of the growth sector, which appears to be rounded towards the main growth direction (arrow labelled α in Fig. 3a, b). In the minor growth direction (β), the less favourable addition of ions (and therefore a ten-fold slower growth) can only start at the corner position **F**, which keeps **F** angular during growth.

We have also calculated that the difference in energy between attaching an SO_4^{2-} ion to a Ba^{2+} ion on the (210) face in the $[1\bar{2}0]$ direction and in the $[\bar{1}20]$ direction is of the order of 1 eV. This explains the anisotropy of the rate for needle growth in these two directions on the (210) plane.

To model two-dimensional nuclei fully would involve an algorithm that dynamically models the statistical attachment of ions and includes the influence of solution composition and defects in the

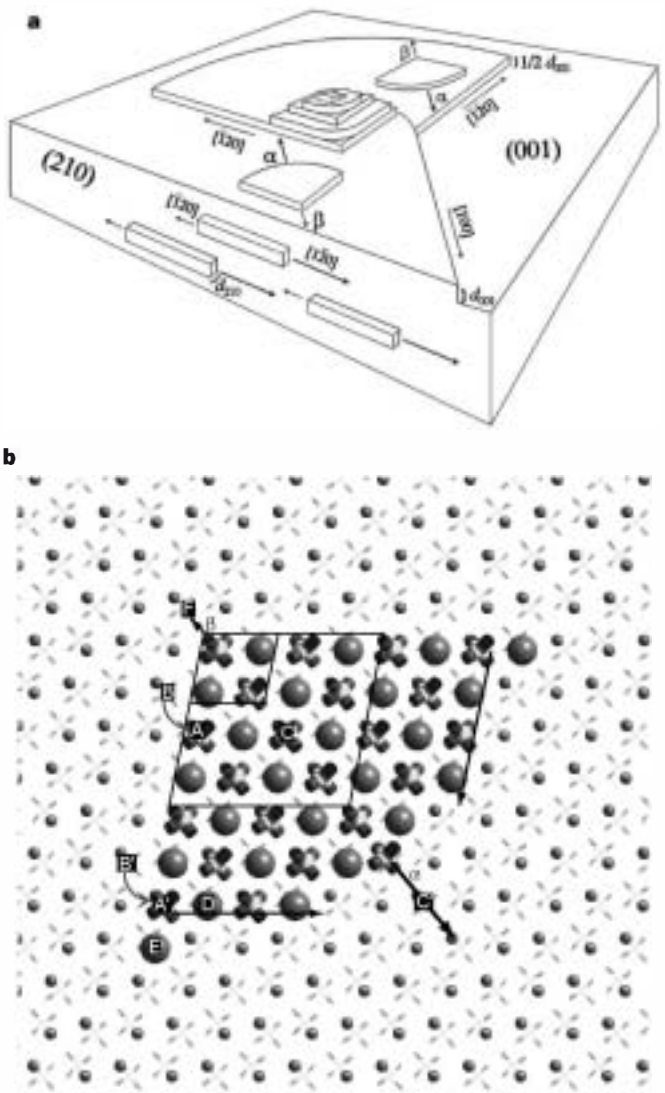

Figure 3 Illustration and computer simulation of crystal growth mechanisms. **a**, Diagram showing the crystallographic orientation of the two-dimensional nuclei on (001) and (210) surfaces, as shown in Figs 1 and 2. The lateral scales on each surface are greatly underestimated relative to the scale normal to the surface. **b**, Computer-simulated image of a sector-shaped, two-dimensional nucleus on a (001) surface. The Ba^{2+} positions and SO_4^{2-} groups are represented by spheres and tetrahedra respectively. The underlying barite substrate is shown in smaller symbols for clarity. The most energetically favourable nucleus (small solid parallelogram), positions of important attachment sites (**A**–**F**) and the growth directions (α, β) are indicated (see text). The microscopic growth directions along the dashed arrows lead to the mesoscopic growth direction α, as observed with AFM. In this image, all molecules outside the larger dashed parallelogram are allowed to relax. The positions **A**, **A′**; **B**, **B′** and so on are symmetry-equivalent in the bulk and define equivalent positions during growth (for example, **A**, **A′** are the starting positions for the growth of a new row).

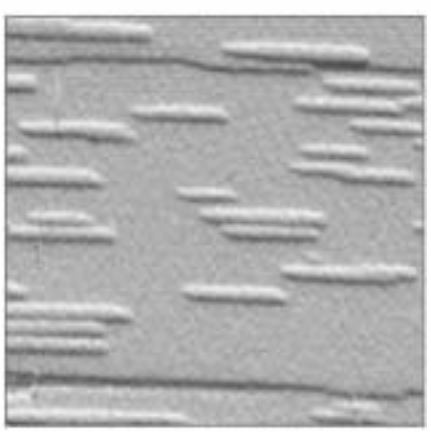

Figure 2 Two-dimensional nucleation on a {210} surface of barite. The nuclei are needle-shaped and grow along ⟨120⟩ directions. The fluid supersaturation value was 19; image area is 1.3 μm × 1.3 μm.

solid[19]. However, the deterministic approach presented here is sufficient to explain the observed anisotropic shape and growth kinetics of the nuclei.

The structural control and anisotropy of the growth explains the inhibition of spiral growth. On the (001) surface, alternate $BaSO_4$ layers are related by a 2_1 screw axis so that the anisotropy and the shape of the nuclei are reversed in each growth layer. The growth of the first $BaSO_4$ layer around the dislocation (Fig. 1b–d) is restricted to one sector, in the α direction (Fig. 3a), and cannot continue around the spiral because of the very slow growth in the opposite β direction. In the next layer that forms around the dislocation, the directions α and β are reversed but the rapid growth along α is almost completely prevented by the very slow growth in the underlying layer in this direction. This alternation of fast and slow directions continues for subsequent layers and so growth around the screw dislocation is limited to an ever-tightening spiral (Fig. 1f). Only when a half-layer from a neighbouring two-dimensional nucleus impinges on the spiral, as in the lower left-hand edge of the spiral in Fig. 1d, can the overlying layer spread laterally.

The {001} and {210} faces dominate the morphology of natural barite crystals, yet the anisotropy of the growth on these faces precludes spiral growth as a kinetically significant process. Only at higher supersaturation, when two-dimensional nucleation becomes a viable mechanism, can the spiral develop laterally. The anisotropy described here is not predicted by any crystal growth theories, principally because they do not take into account the actual surface structure and the attachment energies on specific surface sites. These attachment energies and hence the magnitude of the anisotropy could be modified by the presence of adsorbed impurities. Symmetry criteria allowing anisotropy exist in many crystal structures and therefore it is likely that these results will not only be valid for all compounds[9] having the barite structure, but also more generally. This mechanism of inhibition of spiral growth may explain the "growth-step phenomena" described in other systems[4]. Ultimately, the macroscopic crystal morphology depends on the microscopic processes of adsorption of growth units on crystal faces and step ledges and the methods used here provide powerful tools to observe directly and model these processes. □

1. Chernov, A. A. *Modern Crystallography III (Crystal Growth)* (Springer, Berlin, 1984).
2. Sunagawa, I. in *Morphology of Crystals* (ed. Sunagawa, I.) 323–365 (Terra Scientific, Tokyo, 1987).
3. Burton, W. K., Cabrera, N. & Frank, F. C. The growth of crystals and the equilibrium structures of their surfaces. *Phil. Trans. R. Soc.* **243**, 299–358 (1951).
4. *J. Cryst. Growth* **69**, 182–197 (1984).
5. Bennema, P. & Gilmer, J. in *Crystal Growth: An Introduction* (ed. Hartman, P.) 263–327 (North Holland, Amsterdam, 1973).
6. Botsaris, G. D. in *Industrial Crystallization 81* (eds Jancic, S. J. & de Jong, E. J.) (North Holland, Amsterdam, 1982).
7. Nielsen, A. E. *Kinetics of Precipitation* (Pergamon, Oxford, 1964).
8. Hartman, P. in *Morphology of Crystals* (ed. Sunagawa, I.) 269–319 (Terra Scientific, Tokyo, 1987).
9. Hartman, P. & Strom, C. S. Structural morphology of crystals with the barite ($BaSO_4$) structure: a revision and extension. *J. Cryst. Growth* **97**, 502–512 (1989).
10. Hillner, P. E., Gratz, A. J., Manne, S. & Hansma, P. K. Atomic-scale imaging of calcite growth and dissolution in real time. *Geology* **20**, 359–362 (1992).
11. Dove, P. M. & Chermak, J. in *CMS Workshop Lectures: Scanning Probe Microscopyof Clay Minerals* (eds Nagy, K. L. & Blum, A. E.) 139–170 (Clay Minerals Soc., Washington DC, 1994).
12. Allan, N. L. *et al.* Calculated bulk and surface properties of sulfates. *Faraday Disc.* **95**, 273–280 (1993).
13. Miyaka, M., Minato, I., Morikawa, H. & Iwai, S. Crystal structures and sulphate force constants of barite, celestite and anglesite. *Am. Mineral.* **63**, 506–510 (1978).
14. Hartman, P. & Perdok, W. G. On the relations between structure and morphology of crystals. *Acta Crystallogr.* **8**, 48–52 (1955).
15. Hottenhuis, M. H. J. & Lucasius, C. B. The influence of internal crystal structure on surface morphology; *in situ* observations of potassium hydrogen phthalate {010}. *J. Cryst. Growth* **94**, 708–720 (1989).
16. Hartman, P. & Heijnen, W. M. M. Growth mechanism of a crystal face for which more than one surface structure is possible. *J. Cryst. Growth* **63**, 261–264 (1983).
17. Conway, B. E. *Ionic Hydration in Chemistry and Biophysics* (Elsevier Scientific, Amsterdam, 1980).
18. Rashin, A. A. & Honig, B. Reevaluation of the Born model of ion hydration. *J. Phys. Chem.* **89**, 5588–5593 (1985).
19. Becker, U., Pina, C. M., Risthaus, P., Bosbach, D. & Putnis, A. Experimental and theoretical treatment of molecular-scale mechanisms of crystal growth on barite (Eighth annual V. M. Goldschmidt Conference, Toulouse, France, 1998).

Acknowledgements. We thank the Deutsche Forschungsgemeinschaft (DFG) and the Spanish Ministry of Science and Culture for financial support for this project, and A. Pina for Fig. 3a.

Correspondence and requests for materials should be addressed to A.P. (e-mail: putnis@nwz.uni-muenster.de).